current issues in molecular biology

MDPI

Article

FLS–Macrophage Communication Is Associated with Redox-Related Signaling Networks

Nana Li [1,†], Chonkit Lio [2,3,*,†,‡], Yi Zhu [1], Jie Zeng [4], Yue Zhuo [5], Jinfang Luo [1,*]

[1] Department of Basic Medicine, Department of Pharmacy, Key Laboratory on the Property & Effect of Chinese Medicine (Ethnic Medicine), Guizhou Genuine Herbs Center of Consistency of Utility, The Provincial Key Miao Medicine Laboratory of Guizhou, Guizhou University of Traditional Chinese Medicine, Guiyang 550025, China; linana@stu.gzy.edu.cn (N.L.); zhuyi6695@163.com (Y.Z.)
[2] Faculty of Chinese Medicine, Macau University of Science and Technology, Avenida Wailong, Taipa, Macau, China
[3] State Key Laboratory of Quality Research in Chinese Medicine, Macau University of Science and Technology, Avenida Wailong, Taipa, Macao, China
[4] Natural Products Research Center of Guizhou Province, Guiyang 550014, China; 18485729848@163.com
[5] Science and Technology Innovation Center, Guangzhou University of Chinese Medicine, Guangzhou 510080, China; zhuoyue@gzucm.edu.cn
* Correspondence: thomaslio94@gmail.com (C.L.); luojinfang1@gzy.edu.cn (J.L.)
† These authors contributed equally to this work.
‡ Current address: Department of Medical Biochemistry, Tohoku University Graduate School of Medicine, Sendai 980-8575, Japan

Abstract

Background: Rheumatoid arthritis (RA) involves persistent synovial inflammation together with progressive cartilage damage and bone erosion. Fibroblast-like synoviocytes (FLS) and macrophages are abundant in the inflamed synovium, but how their interactions contribute to matrix-destructive responses is less well defined. Methods: We integrated public bulk and single-cell transcriptomic analyses with experimental validation in collagen-induced arthritis (CIA) tissues to investigate inflammatory, redox-associated, and matrix-remodeling alterations in the RA synovial microenvironment. Bioinformatic analyses, intercellular communication modeling, histological assessment, enzyme-linked immunosorbent assay (ELISA), and immunoblotting were subsequently performed to characterize stromal–immune interactions and Nuclear factor erythroid 2-related factor 2 (NRF2)-associated signaling changes. Results: Single-cell analysis identified synovial immune-cell populations and predicted interactions between fibroblast-like synoviocytes (FLS) and macrophages. CellChat analysis identified extracellular matrix- and inflammatory-associated pathways, including POSTN–integrin and macrophage migration inhibitory factor (MIF)-related signaling, in FLS-to-macrophage communication. Bulk transcriptomic analyses showed higher expression of matrix metallopeptidase 3 (MMP3) and matrix metallopeptidase 13 (MMP13) in RA synovial tissue. RA synovial tissues exhibited elevated expression of matrix metallopeptidase 3 (MMP3) and matrix metallopeptidase 13 (MMP13), while RA macrophages showed increased oxidative stress-associated transcriptional signatures. In CIA rats, increased expression of NRF2-associated antioxidant proteins was accompanied by parallel reduced synovial inflammation and decreased MMP3 and MMP13 expression. Conclusions: These findings suggest that stromal–immune interactions in RA may involve altered macrophage redox regulation associated with matrix-degrading responses. NRF2-associated pathways may therefore contribute to the coordination of inflammatory and tissue-destructive processes in RA.

Academic Editor: Peter C. Hart

Received: 13 September 2026
Revised: 9 November 2026
Accepted: 11 November 2026
Published: 14 November 2026

Copyright: © 2026 by the authors. Licensee MDPI, Basel, Switzerland. This article is an open access article distributed under the terms and conditions of the Creative Commons Attribution (CC BY) license.

Keywords: rheumatoid arthritis; fibroblast-like synoviocytes; macrophages; stromal–immune crosstalk; redox regulation; NRF2; MMP13; matrix degradation

1. Introduction

Synovial inflammation and progressive destruction of cartilage and bone are hallmarks of rheumatoid arthritis (RA) [1,2]. Despite advances in disease-modifying antirheumatic drugs (DMARDs) and biologic therapies, many patients continue to develop structural joint damage during disease progression [3–6]. How inflammatory responses within the RA synovium become linked to matrix-degrading processes—and how these processes differ from the mechanically driven matrix remodeling of osteoarthritis (OA)—remains incompletely defined. Fibroblast-like synoviocytes (FLSs) are major stromal components of the RA synovium and contribute to both inflammatory signaling and tissue remodeling [7,8]. Activated FLS produce inflammatory cytokines and matrix-degrading mediators in response to oxidative stress and pro-inflammatory stimuli, thereby promoting synovial inflammation and joint destruction [9]. In addition to producing cytokines and matrix-associated factors, activated FLS interact extensively with infiltrating immune cells, particularly macrophages, within the inflamed synovial microenvironment [10–12]. Macrophages are abundant in RA synovium and are closely associated with disease severity and joint destruction [13–16]. However, how these interactions mechanistically connect immune activation with matrix degradation remains incompletely understood.

Recent single-cell transcriptomic studies have revealed substantial heterogeneity among synovial stromal and immune-cell populations in RA [17]. These approaches have also identified extensive intercellular signaling networks within the inflamed synovium [18]. In the present study, we integrated bulk and single-cell transcriptomic analyses to systematically characterize the immune landscape and intercellular communication networks within the synovial microenvironment. To further validate the biological findings in vivo, a collagen-induced arthritis (CIA) rat model was employed. JiShe QuShi Capsules (JSQSC) were used as a pharmacological intervention [19], and their major chemical constituents were characterized by ultra-performance liquid chromatography coupled to high-resolution tandem mass spectrometry (UPLC–HRMS/MS; UltiMate 3000 coupled to a Q Exactive Focus hybrid quadrupole-Orbitrap mass spectrometer). Notably, although MMP3, MMP13, and POSTN are also implicated in OA cartilage degradation, in RA these mediators are predominantly produced by activated synovial fibroblasts and infiltrating myeloid cells within an inflamed synovium, a cellular context distinct from OA. Overall, this study aimed to elucidate the crosstalk among stromal–immune interactions, redox-associated signaling pathways, and matrix-degradative responses in the RA synovium.

2. Materials and Methods

2.1. Public Transcriptomic Datasets and Bioinformatic Analysis

Publicly available RA synovial transcriptomic datasets, including GSE55235, GSE77298, GSE55457, and GSE246416, were downloaded from the Gene Expression Omnibus (GEO) database. The bulk datasets GSE55235, GSE77298 and GSE55457 were analyzed separately using the limma package (v3.62.2) in R to screen for differential gene expression between RA and control synovial samples. Disease status (RA versus control) was used as the grouping variable, and no additional covariates were included. Differentially expressed genes (DEGs) were identified using thresholds of $p < 0.05$ and $|\log2FoldChange| > 1.5$. Nominal p values were used for the initial exploratory screening. For the

complete limma results reported in Supplementary Table S4, Benjamini–Hochberg correction was applied across all tested genes separately within each dataset. Directional concordance was distinguished from corrected significance at FDR < 0.05. Results from these three independent bulk datasets were subsequently compared to assess cross-dataset consistency. Table 1 provides detailed information on each dataset.

Single-cell RNA-sequencing data comprised five healthy-control samples from GSE246416 [20], and four RA samples from GSE200815 [21]. The single-cell datasets GSE246416 and GSE200815 were analyzed using Seurat package (v4.3.0) in R for cell-type characterization, pathway-level analyses, and intercellular communication analysis. Cells expressing fewer than 200 genes or showing >20% mitochondrial transcripts were excluded during quality control, and genes detected in fewer than three cells were removed. After quality-control filtering, 82,077 cells from nine samples, including five control and four RA samples, were retained for downstream analysis. Total retained cell numbers, quality-control summaries, and the numbers of each cell population included in the CellChat input are provided for each donor in Table S2. Samples were normalized with SCTransform, and integration features were identified using SelectIntegrationFeatures. Datasets were merged through Seurat reference-based SCT anchor integration, employing FindIntegrationAnchors and IntegrateData. Principal component analysis (PCA) and uniform manifold approximation and projection (UMAP) were then applied for dimensionality reduction and visualization. Cell clusters were identified using a shared nearest-neighbor graph–based approach with the first 20–30 principal components. Immune-cell labels used in downstream analyses were assigned using marker-based scores, with cluster-level SingleR (v2.4.1) results from multiple reference datasets providing complementary annotations. All retained cells, including stromal and immune cells, were included in the initial integration and clustering. For CellChat analysis, putative FLS were identified from the full-cell object based on expression of COL1A1, COL1A2, DCN, LUM, PDPN, and THY1. The FLS marker score was calculated as the mean log-normalized expression of these markers. Cells lacking an assigned immune-cell label, with undetectable PTPRC expression, and with an FLS score above the 90th percentile of the full-cell score distribution were selected. This operational definition identified a high-marker-expression fibroblast compartment, rather than providing a comprehensive annotation of all stromal cells. Macrophages were assigned using marker-based scores incorporating C1QA, C1QB, C1QC, APOE, TREM2, MSR1, and CTSD. Marker expression supporting these annotations is shown in Supplementary Figure S2. The numbers of FLS, macrophages, and other cell populations included in the CellChat input are provided for each donor in Table S2. Other stromal populations were not comprehensively subclassified, and cells without an immune-cell assignment that did not meet the FLS criteria were excluded from this communication analysis.

Transcriptional program scores were calculated from the RNA assay after Seurat LogNormalize normalization with a scale factor of 10,000. Each per-cell score was the mean log-normalized expression of the available gene-set members, without background-control gene subtraction. Complete gene lists, their sources and selection rationale, and genes present or missing from the analyzed matrix are provided in Supplementary Table S3. For Figure 1B, per-cell transcriptional program scores were summarized as the median within each donor and annotated cell type. Individual donors, rather than individual cells, constituted the units displayed. These comparisons were descriptive; no inferential statistical tests were applied to the scores shown. For macrophage-specific differential-expression analysis, raw RNA counts were aggregated at the donor level to generate pseudobulk count matrices, with individual donors treated as biological replicates. Lowly expressed genes were filtered using edgeR filterByExpr, followed by normalization using

calcNormFactors. Differential expression between RA and control macrophage pseudobulk samples was assessed using edgeR (v4.0.16) with the quasi-likelihood framework. Disease status was included as the explanatory variable, with no additional covariates. Multiple testing was controlled using the false discovery rate reported by edgeR.

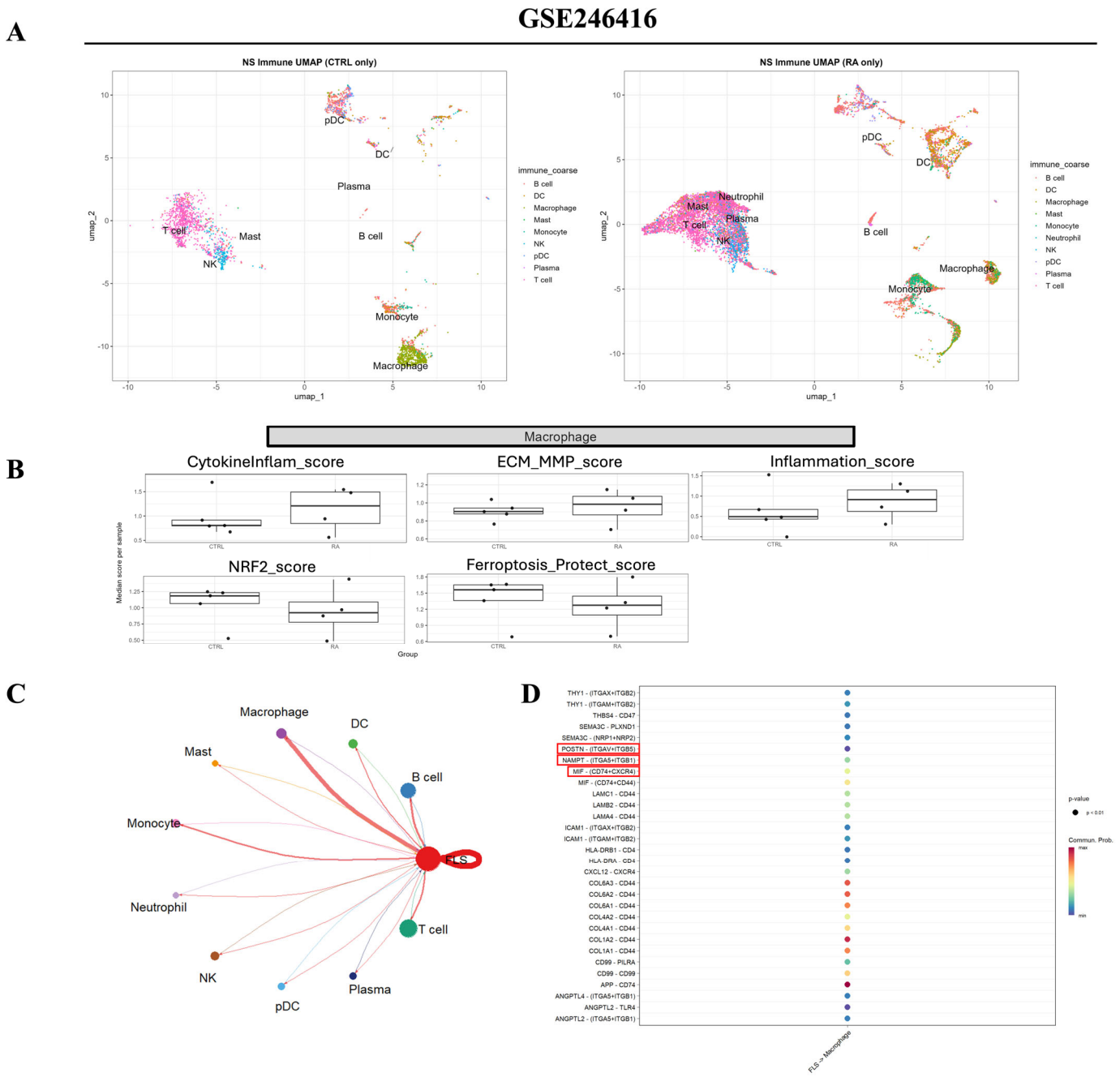


Figure 1. RA synovial immune remodeling and FLS–macrophage communication are associated with inflammatory and redox-related programs. (**A**) UMAP visualization of annotated synovial cell populations in RA and control samples. (**B**) Pathway activity analysis demonstrating enhanced inflammatory, extracellular matrix-matrix metallopeptidase-related (ECM–MMP–related), and redox-associated signatures in RA macrophages. Each point represents the median score for one donor within the indicated cell type. Comparisons are descriptive, without inferential statistical testing. (**C**) CellChat analysis of the combined RA and control dataset, showing inferred intercellular communication. (**D**) Predicted FLS-to-macrophage ligand–receptor interactions in the combined dataset, including POSTN–integrin, NAMPT–integrin, and MIF– (CD74 + CXCR4) interactions.

Table 1. Summary of the GEO datasets included in this study.

Dataset ID	Platform	RA		Control	
		Type	Number	Type	Number
GSE55235	GPL96	Synovium	10	Synovium	10
GSE77298	GPL570	Synovium	16	Synovium	7
GSE55457	GPL96	Synovium	13	Synovium	10
GSE246416	GPL24676	Synovium	0	Synovium	5
GSE200815	GPL24676	Synovium	4	Synovium	0

2.2. Cell–Cell Communication Analysis

Cell–cell communication analysis was conducted using the CellChat package (v1.6.1). Normalized single-cell expression matrices together with annotated cell identities were used as input, and ligand–receptor interactions were inferred based on the CellChatDB database. Communication probabilities were calculated using the default CellChat statistical framework with population-size adjustment. A minimum threshold of 10 cells per cell population was applied; cell populations containing fewer than 10 cells were excluded from downstream analysis, and inferred interactions were further filtered using filterCommunication with min.cells = 10. Interactions with $p < 0.05$ were retained for downstream analysis. Pathway-level communication probabilities were subsequently calculated and aggregated. RA and control samples were analyzed within a combined CellChat object; therefore, the analysis was used to characterize the overall inferred communication network rather than to directly compare communication probabilities between the two conditions.

Incoming and outgoing signaling activities were compared across major synovial cell populations to identify dominant signaling sources and target cells within the RA microenvironment. Pathways related to inflammatory activation and extracellular matrix remodeling, including Periostin (POSTN), Macrophage Migration Inhibitory Factor (MIF), and nicotinamide phosphoribosyltransferase (NAMPT) signaling, were further examined. Communication networks were visualized using CellChat-generated heatmaps, circle plots, and bubble plots.

2.3. Reagents and Antibodies

JiShe QuShi Capsules (JSQSC; Approval Number: Qian Yao Zhi Zi Z20160028; Batch No. 20221001; Specification: 0.45 g × 36 capsules) were provided by the Department of Rheumatology and Immunology, Second Affiliated Hospital of Guizhou University of Traditional Chinese Medicine. JSQSC is a proprietary Chinese medicine formulation composed of processed Rhizoma Cibotii 15 g, Zaocys 10 g, Rhizoma Homalomenae 15 g, Periploca forrestii Schltr. 10 g, Caulis Sinomenii 15 g, Notoginseng Powder 6 g, Rhizoma Curcumae Longae 9 g, Radix Paeoniae Alba 12 g, and Radix et Rhizoma Glycyrrhizae 6 g. The capsules were stored in a dry place at room temperature (25 °C). Doses of JSQSC were extrapolated from human clinical exposure to rats using an interspecies conversion factor of 6.3. The medium dose (0.49 g/kg) represents the calculated clinical equivalent; the low (0.16 g/kg) and high (1.47 g/kg) doses were scaled to one-third and threefold this equivalent, respectively, for dose–response assessment. For administration, the capsule contents were suspended in saline at concentrations of 0.016, 0.049, and 0.147 g/mL, corresponding to low-, medium-, and high-dose treatments of 0.16, 0.49, and 1.47 g/kg, respectively.

Complete Freund's adjuvant (Cat. No. 210154) and bovine type II collagen (Cat. No. 20022) were purchased from Chondrex (Redmond, WA, USA). Methotrexate (MTX; Cat. No. 517B021) was obtained from Solarbio (Beijing, China).

Primary antibodies against microsomal prostaglandin E synthase-1 (mPGES-1), NRF2, heme oxygenase-1 (HO-1), glutathione peroxidase 4 (GPX4), MMP3, MMP13, and β-actin were obtained from Agrisera (Vännäs, Sweden), Hua'an Biotechnology (Hangzhou, China), Proteintech (Wuhan, China), and Affinity Biosciences (Cincinnati, OH, USA). HRP-conjugated secondary antibodies were obtained from Wuhan Doctor Biological Engineering Co., Ltd. (Wuhan, China). Detailed antibody information, including manufacturers, catalogue numbers, and working dilutions, is provided in Table 2.

ELISA kits for tumor necrosis factor-α (TNF-α), interleukin-6 (IL-6), interleukin-1β (IL-1β), and prostaglandin E2 (PGE2) were purchased from MultiSciences Biotech (Hangzhou, China) and Cayman Chemical (Ann Arbor, MI, USA). RIPA lysis buffer, BCA protein assay kits, SDS–PAGE reagents, transfer buffers, and other immunoblotting reagents were obtained from commercial suppliers.

Table 2. Summary of the detailed antibody information.

Antibody Name	Manufacturer	Catalogue Number	Dilution Ratio (Antibody: Diluent)	Immunogen	Species Specificity
mPGES-1	Agrisera	AS03031	1:1000	Recombinant human purified 6-His mPGES-1 O14684	Human, Mouse, Rat, sheep
NRF2	Affinity Biosciences	AF0639	1:1000	A synthesized peptide derived from human Nrf2, corresponding to an amino-terminal region	Human, Mouse, rat
HO-1	Wuhan Sanying Biotechnology Co., LTD.	10701-1-AP	1:2000	Recombinant human HMOX1 protein (AG1190)	Human, mouse, rat
GPX4	Wuhan Sanying Biotechnology Co., LTD.	30388-1-AP	1:1000	Recombinant human GPX4 protein (AG30650)	Human, mouse, rat
MMP13	Affinity Biosciences	AF5355	1:1000	A synthesized peptide derived from human MMP13, corresponding to a region within N-terminal amino acids	Human, mouse, rat
MMP3	Affinity Biosciences	AF0217	1:2000	A synthesized peptide derived from human MMP3, corresponding to a region within C-terminal amino acids.	Human, mouse, rat
β-actin	Wuhan Sanying Biotechnology Co., LTD.	66009-1-Ig	1:2000	Recombinant human β-actin protein (Clone 2D4H5)	Human, mouse, rat, pig, rabbit, canine, monkey, chicken, zebrafish, hamster
Horseradish peroxidase (HRP)-labeled mouse secondary antibody	Wuhan Doctor Biological Engineering Co., LTD.	BA1051	1:3000	mouse IgG (whole molecular)	mouse IgG
Horseradish peroxidase (HRP)-labeled rabbit	Wuhan Doctor Biological Engineering Co., LTD.	BA1054	1:3000	Rabbit IgG (whole molecular)	Rabbit IgG

secondary antibody	

2.4. Chemical Profiling of JSQSC by UPLC–HRMS/MS

Chemical constituents of JSQSC were characterized using an UltiMate 3000 UHPLC system coupled with a Q Exactive Focus hybrid quadrupole–Orbitrap mass spectrometer (Thermo Fisher Scientific, USA). Chromatographic separation was performed on an ACE UltraCore Super C18 column (100 × 2.1 mm, 2.5 μm) using a mobile phase consisting of 0.1% formic acid in water and acetonitrile under gradient elution. The flow rate was maintained at 0.3 mL/min, and the column temperature was set at 40 °C.

Mass spectrometric data were acquired in both positive and negative ion modes over a scan range of m/z 100–1500. Compound identification was performed using Xcalibur and Compound Discoverer 3.2 software (Thermo Fisher Scientific, USA) by comparison with an in-house traditional Chinese medicine database and the mzCloud database.

2.5. Experimental Animals and CIA Induction

Sprague–Dawley rats (6–7 weeks old, 160–180 g, male) were obtained from Beijing HFK Bioscience Co., Ltd. (Experimental Animal Production License No. SCXK (Jing) 2021-0003). The animals were housed in an accredited animal facility (Experimental Animal Use License No. SYXK (Qian) 2021-0005) under controlled conditions (temperature 22 ± 2 °C, humidity 50–60%, 12-h light/dark cycle) with free access to standard chow and water. After a one-week acclimatization period, rats were randomly assigned to experimental groups prior to CIA induction. Animal experiments were approved by the Ethics Review Committee of Animal Experiments, Guizhou University of Traditional Chinese Medicine (Approval No. 20220090; approval date: 1 August 2022).

CIA was established as previously described. Briefly, bovine type II collagen was emulsified with complete Freund's adjuvant and administered by intradermal injection at the base of the tail on days 1 and 7. Control rats received an equal volume of saline. Rats that showed no signs of arthritis by day 14 post-immunization were excluded from the study. Throughout the experimental period, rats were euthanized if paw swelling exceeded 50% of baseline, body weight loss exceeded 20%, or severe ulceration was observed; however, no adverse events requiring early euthanasia occurred. At the end of the study, all surviving animals were euthanized by cervical dislocation.

A total of 36 rats were used ($n = 6$ per group). The sample size of $n = 6$ per group was determined based on previously published collagen-induced arthritis studies. At day 35, the primary comparison (Model versus Control) showed: arthritis score, Cohen's d = 5.24 (95% CI: 2.69–7.79); paw swelling, Cohen's d = 4.91 (95% CI: 2.48–7.34). This sample size was adequate to detect biologically meaningful differences. Rats were randomly allocated to six groups using a computer-generated randomization sequence (Microsoft Excel RAND function) stratified by body weight to ensure comparable baseline characteristics across groups: control, CIA model, MTX, and low-dose, medium-dose, and high-dose JSQSC groups. From day 14 after immunization, JSQSC was administered orally once daily at doses of 0.16, 0.49, and 1.47 g/kg, respectively. MTX-treated rats received methotrexate (1 mg/kg) once weekly. Control and model groups received an equal volume of saline (this experiment followed the ARRIVE guidelines 2.0).

2.6. Clinical Assessment and Histological Analysis

Paw swelling and arthritis scores were recorded weekly throughout the experimental period and assessed independently by two investigators blinded to group allocation. After treatment, knee joint tissues were collected, fixed in 4% paraformaldehyde for 48 h, decalcified in 10% EDTA for 21 days, embedded in paraffin, and sectioned (5 μm). Sections

were stained with hematoxylin and eosin (H&E) for morphological evaluation. Scale bars = 200 μm.

2.7. ELISA

Serum samples were collected after the final treatment. The levels of TNF-α, IL-6, IL-1β, and PGE_2 were determined using commercial ELISA kits according to the manufacturers' instructions.

2.8. Western Blot Analysis

At the endpoint, three of the six rats per group were selected at random for synovial tissue collection for Western blotting. Synovial tissues were homogenized in RIPA lysis buffer containing protease inhibitor cocktail and phosphatase inhibitors. Protein concentrations were determined using a BCA protein assay kit. Equal amounts of protein (30 μg per lane) were separated by 10% SDS-PAGE and transferred onto 0.45 μm PVDF membranes at 300 mA for 90 min. Membranes were blocked in 5% non-fat milk in TBST for 1 h at room temperature, then incubated overnight at 4 °C with primary antibodies: mPGES-1, NRF2, HO-1, GPX4, MMP3, MMP13, and anti-β-actin. After washing, membranes were incubated with HRP-conjugated secondary antibodies for 1 h at room temperature. Due to the broad molecular weight range of the target proteins and to avoid potential artifacts from antibody stripping, all proteins were detected without stripping and reprobing. Protein bands were visualized using ECL substrate and imaged on a ChemiDoc system. Densitometric quantification was performed using ImageJ v1.53k (n = 3 represents three biologically independent animals per group).

2.9. Statistical Analysis

Data are presented as mean ± standard deviation. For longitudinal data including paw swelling and arthritis scores, two-way repeated-measures ANOVA was performed with Group as the between-subjects factor and Time as the within-subjects factor. Mauchly's test indicated violation of sphericity for both paw swelling and arthritis scores; therefore, degrees of freedom were corrected using the Greenhouse–Geisser method (ε = 0.740 for paw swelling and ε = 0.712 for arthritis scores). Post hoc pairwise comparisons were performed using Tukey's test for between-group comparisons at each time point. Differences among groups were analyzed using one-way ANOVA followed by Tukey's multiple-comparisons test. Genome-wide differential expression of the bulk datasets was assessed using limma as described in Section 2.1; the Wilcoxon rank-sum tests shown in Figure 2B are descriptive comparisons of expression distributions only and do not constitute independent validation of the same data. All biochemical assessments were conducted by investigators blinded to group allocation; tissue samples and serum aliquots for ELISA and Western blot were coded by an independent researcher prior to analysis. A value of $p < 0.05$ was considered statistically significant. Analyses were performed using SPSS 26.0 and GraphPad Prism 9.

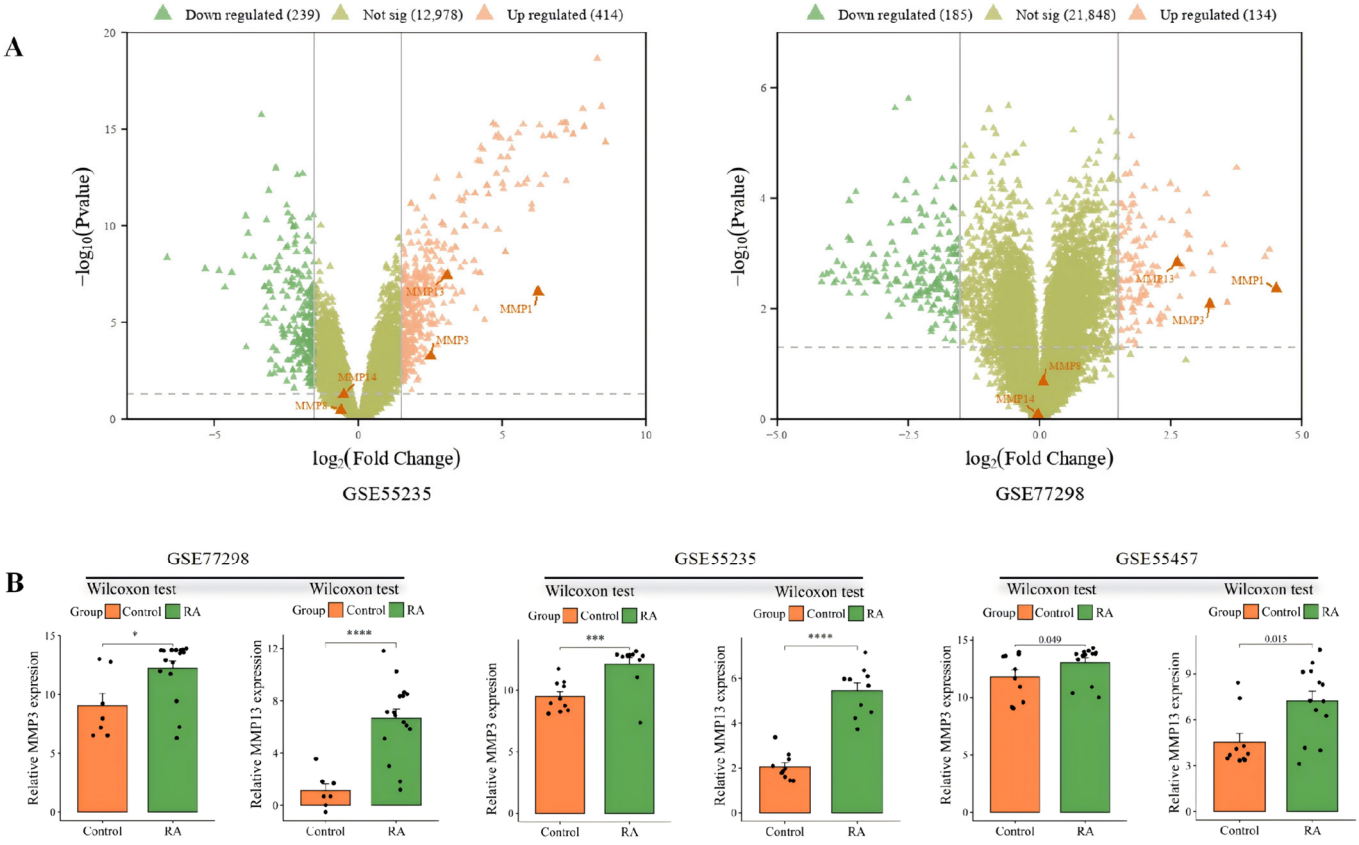


Figure 2. MMP3 and MMP13 are consistently elevated in RA synovium and associated with matrix-destructive programs. (**A**) Differential-expression analysis of the bulk GEO datasets using limma, with $p < 0.05$ and |log2 fold change| > 1.5 used for classification in the volcano plots. (**B**) Expression levels of MMP3 and MMP13 in the individual bulk datasets. Wilcoxon rank-sum tests were used specifically for the targeted RA-versus-control comparisons shown in panel B: * $p < 0.05$, *** $p < 0.001$, and **** $p < 0.0001$.

3. Results

3.1. Altered Immune Landscape in RA Synovium

Single-cell transcriptomic analysis revealed a markedly altered immune landscape in RA synovial tissues compared with controls. The UMAP visualization displays the distribution of annotated immune-cell populations in RA and control samples (Figure 1A). Marker-based annotation classified 11 of 35,609 cells retained after quality control in the RA dataset (GSE200815) and 0 of 46,468 cells in the healthy-control dataset (GSE246416) as putative neutrophils. Given the small counts and the confounding of disease status with study of origin, these observations do not establish neutrophil expansion in RA.

3.2. Inflammatory Signaling Is Coupled with Matrix Remodeling in RA

To investigate the relationship between inflammatory activation and tissue-destructive responses in macrophages, we compared pathway activity scores between RA and CTRL samples. RA macrophages exhibited increased inflammatory signaling, including elevated cytokine/inflammatory response scores, ECM–MMP–related activity, and oxidative stress–associated signatures (Figure 1B). Pathways related to matrix remodeling were also enriched in RA macrophages, consistent with enhanced tissue-destructive activity in the RA synovial microenvironment.

3.3. FLS–Macrophage Crosstalk Is Associated with Redox-Related Signaling Networks

FLS are known to contribute to the inflammatory and stromal microenvironment in RA. To characterize potential intercellular communication within the synovium, we performed CellChat analysis on the combined RA and control dataset. The predicted interactions describe the pooled dataset and do not establish RA-specific changes or increased communication in RA. FLS were identified as a major source of inferred outgoing signaling and exhibited predicted interactions with multiple immune cell populations, particularly macrophages (Figure 1C).

Ligand–receptor analysis of predicted FLS-to-macrophage communication identified extracellular matrix–integrin interactions and inflammatory signaling pathways, including POSTN–integrin, NAMPT–integrin, and MIF–(CD74 + CXCR4) signaling axes (Figure 1D). These pathways have been implicated in inflammatory activation and metabolic or redox regulation, suggesting potential communication routes between FLS and macrophages within the synovial microenvironment.

POSTN, MIF, and NAMPT were highlighted because they ranked among the prominent predicted FLS-to-macrophage signaling pathways and have been implicated in RA-related inflammation, extracellular matrix remodeling, and metabolic regulation.

3.4. Interstitial Collagenases, Including MMP3 and MMP13, Are Consistently Elevated in RA

To identify mediators associated with matrix degradation in RA without selection bias, we examined the expression of all major interstitial collagenases and related MMPs, namely MMP1, MMP3, MMP8, MMP13, and MMP14, across the synovial transcriptomic datasets. MMP8, the prototypical neutrophil-derived collagenase, was included to represent the neutrophil arm of matrix degradation. Whereas MMP3 and MMP13 were significantly upregulated, MMP8 and MMP14 showed no significant change in either bulk dataset (Figure 2A,B). Across the three bulk synovial datasets, MMP8 had negative log2 fold changes in GSE55235 and GSE55457 and a positive log2 fold change in GSE77298; none met FDR < 0.05 (Table S4). Bulk MMP8 expression does not establish neutrophil abundance or identify the cellular source of the signal. These findings are consistent with increased matrix-remodeling activity in RA synovial tissues.

3.5. Pharmacological Modulation Attenuates Arthritis Progression and Inflammatory Responses In Vivo

To evaluate the in vivo relevance of the proposed stromal–immune regulatory network, pharmacological modulation was examined in a CIA model. Two-way repeated-measures ANOVA revealed significant main effects of treatment group (paw swelling: $F(5, 30) = 38.96$, $p < 0.0001$; arthritis scores: $F(5, 30) = 54.37$, $p < 0.0001$) and time (foot swelling: $F(2.220, 66.61) = 13.16$, $p < 0.001$; arthritis scores: $F(2.137, 64.10) = 76.98$, $p < 0.001$, Greenhouse–Geisser corrected), as well as significant group × time interactions (foot swelling: $F(15, 90) = 2.63$, $p = 0.0025$; arthritis scores: $F(15, 90) = 6.996$, $p < 0.0001$). Mauchly's test indicated violation of sphericity for both endpoints ($W = 0.318$ and 0.187, respectively, both $p < 0.001$). Significant differences are indicated as * $p < 0.05$, ** $p < 0.01$ and *** $p < 0.001$. Treatment reduced paw swelling and arthritis scores in a dose-dependent manner, with effects comparable to methotrexate treatment (Figure 3A–J). H&E staining revealed qualitatively reduced synovial hyperplasia and inflammatory cell infiltration in the treatment groups compared with the CIA model group (Figure 3K). These histological observations are descriptive only.

In parallel, decreased levels of pro-inflammatory cytokines, including TNF-α, IL-6, IL-1β, and PGE_2, were observed following treatment (Figure 3L–O), suggesting attenuation of inflammatory responses within the synovial microenvironment. Chemical profiling identified multiple candidate bioactive constituents associated with JSQSC (Table S1).

Representative chromatographic fingerprints and major compounds were further characterized by UPLC–HRMS/MS analysis (Figure S1A–C). This analysis serves as a characterization of the formulation.

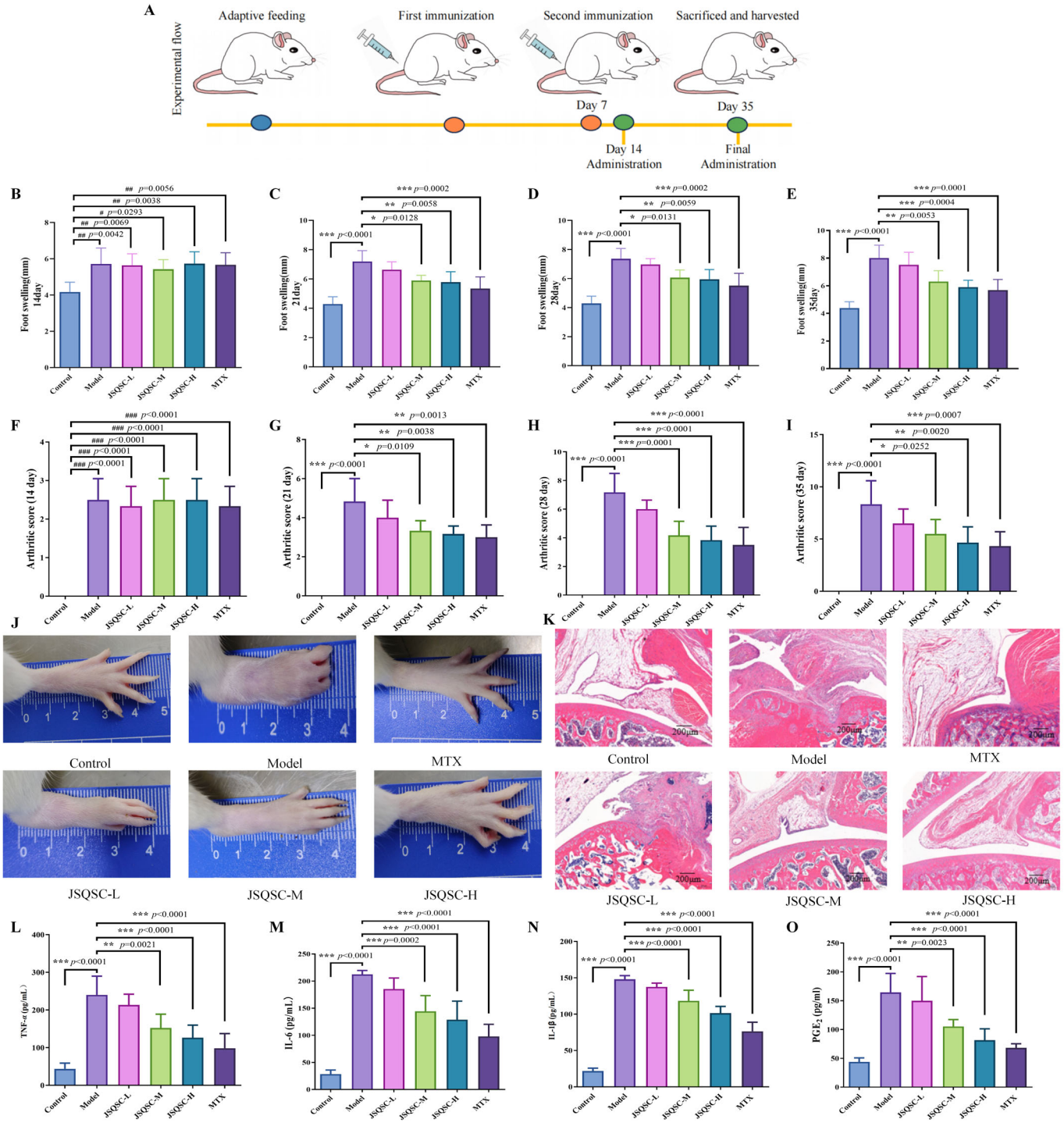


Figure 3. Pharmacological modulation attenuates inflammatory and matrix-destructive responses in CIA rats. (**A**) Schematic illustration of CIA induction, JiShe QuShi Capsules (JSQSC) administration, and experimental sample collection. (**B–E**) Quantitative analysis of paw swelling in different treatment groups during disease progression. Data are presented as mean ± SD (n = 6 per group). * $p < 0.05$, ** $p < 0.01$, *** $p < 0.001$ versus model group; $^{\#}p < 0.05$, $^{\#\#}p < 0.01$ versus control group. The exact p-value is shown in the figure. (**F–I**) Arthritis scores in different treatment groups during the experimental period. Data are presented as mean ± SD (n = 6 per group). * $p < 0.05$, ** $p < 0.01$, *** $p < 0.001$ versus model group; $^{\#\#\#}p < 0.001$ versus control group. The exact p-value is shown in the

figure. (**J**) Representative photographs of hind paws from each group at the endpoint, illustrating paw swelling and joint deformity. (**K**) Representative images of hematoxylin and eosin (H&E)-stained synovial tissues from different treatment groups, showing changes in paw morphology, synovial hyperplasia, and inflammatory cell infiltration. (**L**–**O**) Serum levels of pro-inflammatory mediators measured by ELISA: (**L**) tumor necrosis factor-α (TNF-α), (**M**) interleukin-6 (IL-6), (**N**) interleukin-1β (IL-1β), and (**O**) prostaglandin E_2 (PGE_2). Data are presented as mean ± SD (n = 6 per group). ** $p < 0.01$, *** $p < 0.001$ versus model group.

3.6. Pharmacological Modulation Increases NRF2-Related Protein Expression and Is Associated with Reduced MMP Levels

After we confirmed the attenuation of inflammatory responses within the synovial microenvironment, we next explore the involvement of redox-related pathways. We examined the effects of pharmacological modulation on NRF2-associated signaling in vivo. JSQSC treatment increased the expression of NRF2 and its associated antioxidant proteins, including HO-1 and GPX4, in synovial tissues (Figure 4A–E). On the other hand, the expression of MMP3 and MMP13 was also decreased after JSQSC treatment (Figure 4F–G). Emerging evidence suggests that activation of the NRF2/HO-1 antioxidant pathway suppresses matrix-degrading enzymes such as MMP13 and protects cartilage integrity under inflammatory and oxidative stress conditions. Together, this evidence suggests a link between NRF2-associated redox regulation and MMP expression in RA synovial tissues.

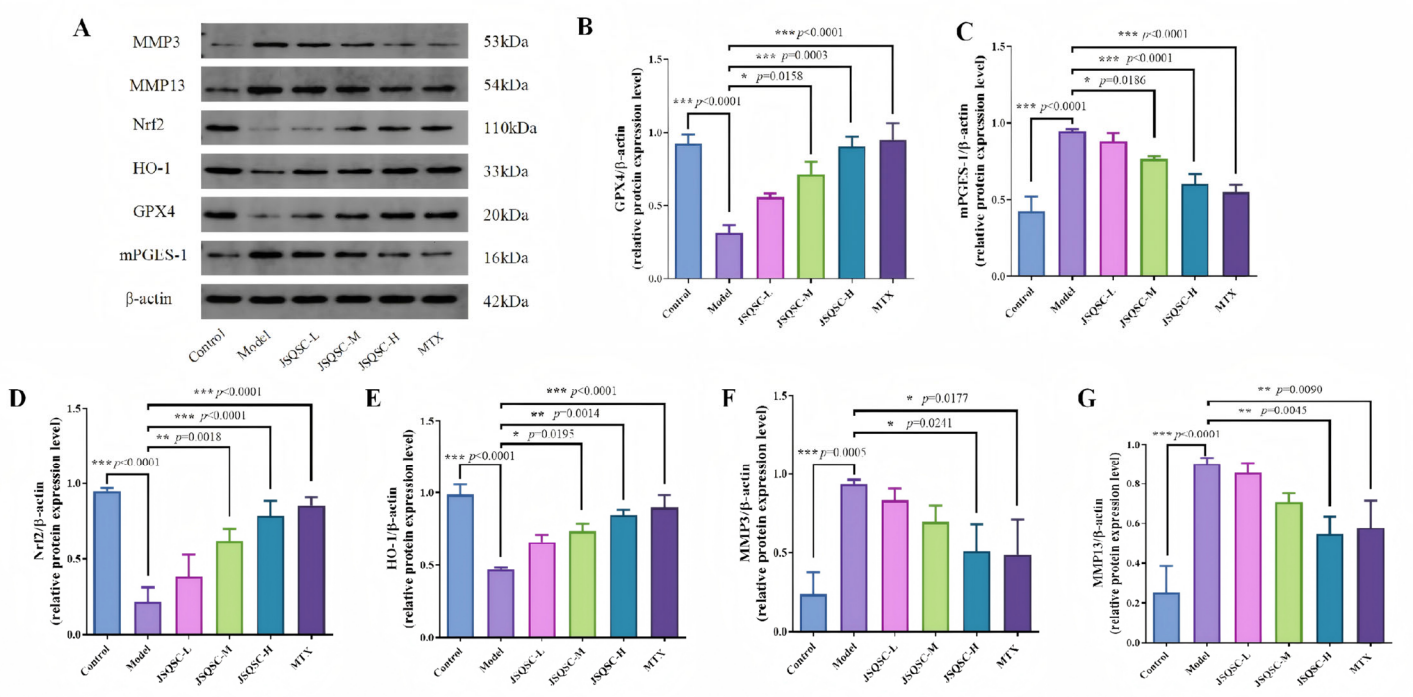


Figure 4. Pharmacological modulation increases NRF2-associated protein expression and is associated with decreased matrix-degrading protein expression in CIA rats. (**A**) Representative Western blot analysis of MMP3, MMP13, Nrf2, HO-1, GPX4 and mPGES-1 expression in synovial tissues from different treatment groups. (**B**–**G**) Quantification of protein expression levels normalized to β-actin. Data are presented as mean ± SD (n = 3 represents three biologically independent animals per group). * $p < 0.05$, ** $p < 0.01$, *** $p < 0.001$ versus model group. The exact p-value is shown in the figure.

4. Discussion

Persistent synovial inflammation in RA is accompanied by progressive destruction of cartilage and bone but the mechanisms linking inflammatory activation to matrix-degrading responses remain unclear. Transcriptomic analyses identified predicted FLS–macrophage interactions and characterized inflammatory, matrix-remodeling, and redox-related transcriptional programs [22]. Elevated expression of MMP3 and MMP13—produced mainly by FLS and macrophages rather than chondrocytes as in OA—was consistently observed in RA synovial tissues, suggesting an inflammation–matrix remodeling axis that is spatially and cellularly distinct from the cartilage-centered MMP response of OA [23–25]. We also observed signaling interactions between FLS and macrophages in RA synovium, including POSTN–integrin and MIF-associated pathways previously implicated in RA inflammation. Our findings identify predicted signaling links between FLS and macrophages that may be relevant to macrophage inflammatory states within the synovial microenvironment. However, this inference requires direct experimental validation of specific ligand–receptor pathways, such as POSTN–integrin and MIF–(CD74 + CXCR4).

NRF2 is a major regulator of cellular antioxidant responses and has been implicated in inflammatory regulation in several chronic diseases [26]. In CIA rats, JSQSC treatment was associated with increased NRF2, HO-1, and GPX4 expression, together with reduced synovial inflammation and decreased MMP3 and MMP13 expression. However, these findings do not demonstrate NRF2 transcriptional activation or direct regulation of MMP3 and MMP13. The reduced MMP expression may instead be secondary to the overall decrease in inflammation. Further studies using NRF2 nuclear translocation, redox assays, and pharmacological or genetic inhibition are required to establish causality [27].

The interactions between FLS and macrophages described here were inferred primarily from transcriptomic analyses and have not yet been directly validated experimentally. The CIA experiments provide tissue-level evidence that inflammatory, redox-related, and matrix-degrading changes occur concurrently in vivo; however, they do not directly validate the cell-specific FLS–macrophage interactions inferred from the human transcriptomic data. In addition, the CIA model cannot fully recapitulate the cellular complexity of human RA synovium [28]. Direct links between macrophage redox alterations and matrix degradation remain unresolved. Together, our findings suggest that RA synovial tissues exhibit concurrent inflammatory, redox-associated, and matrix-remodeling changes accompanied by enriched inferred communication between FLS and macrophages.

Several limitations should be noted. Bulk synovial tissue expression changes do not identify their cellular source or establish FLS and macrophages as the predominant producers of MMPs. The transcriptional program scores were evaluated descriptively and do not directly measure oxidative stress or pathway function. The gene-level pseudobulk analysis did not directly test these scores and therefore cannot be considered confirmation of the observed score differences. Changes in NRF2, HO-1, GPX4, MMP3, and MMP13 may partly reflect reduced inflammation rather than a direct NRF2-dependent effect. All healthy control single-cell samples were obtained from GSE246416, while all RA samples were sourced from GSE200815. Consequently, disease status was confounded with study origin. The 90th-percentile FLS-score threshold selected a high-marker-expression fibroblast compartment and may have favored an extracellular matrix-rich subset, influencing the inferred communication pathways. CellChat pooled cells without equalizing donor contributions; therefore, donors with greater representation within a cell population may have disproportionately influenced the inferred network. Despite the application of a standardized processing and integration workflow, residual study-specific effects could not be distinguished from disease-related differences. Therefore, comparisons between

RA and control groups were considered exploratory. Additionally, the CIA model does not fully replicate human RA. Neutrophils were rarely detected in the exploratory analysis, which prevented reliable assessment of their abundance or MMP expression. This observation should not be interpreted as evidence for their absence in the original tissue. Edalat et al. identified a small neutrophil population in freshly dissociated synovial tissue and discussed limitations in their recovery and detection by scRNA-seq [22]. Therefore, this analysis cannot rule out neutrophil involvement or determine the predominant cellular source of MMPs. Neutrophils were not specifically quantified in the collagen-induced arthritis experiments, leaving their contribution in this model unresolved. Their contribution to MMP production and joint pathology therefore remains unresolved. In addition, the CellChat-predicted interactions and the NRF2–MMP relationship require further experimental validation.

5. Conclusions

This study identifies associations among inferred FLS–macrophage communication, inflammatory and redox-related changes, and MMP expression in RA. Integrated transcriptomic analyses together with pharmacological modulation in vivo suggest that these processes may be linked within the synovial microenvironment. Further mechanistic studies are required to establish causality and determine whether these associations have therapeutic relevance.

Supplementary Materials: The following supporting information [29] can be downloaded at: https://www.mdpi.com/article/10.3390/cimb48111220/s1.

Author Contributions: N.L. and C.L.: methodology, resources, formal analysis, software, project administration, and writing—original draft. Y.Z. (Yi Zhu): data curation, formal analysis, and validation. J.Z. and Y.Z. (Yue Zhuo): data curation and investigation. C.L. and J.L.: writing—review, editing and resources. All authors have read and agreed to the published version of the manuscript.

Funding: This paper was supported by the Basic Research Program of Guizhou Science and Technology Plan Project (Project No.: Qian ke he ji chu-ZK [2022] Yi ban 477); Research Project of Guizhou University of Traditional Chinese Medicine: No. Gui Zhong Yi Ke Yu (2025)54; Guizhou University of Traditional Chinese Medicine Talent Innovation Team [Gui Traditional Chinese Medicine TD He Zi [2023] 002]; Guizhou University of Traditional Chinese Medicine National and Provincial Science and Technology Innovation Talent Team Cultivation Project (Guizhou University of Traditional Chinese Medicine TD NO.[2022]004); Guizhou Provincial Basic Research Program(No.MS [2025] 182).

Institutional Review Board Statement: All animal experiments were conducted in accordance with the institutional guidelines for the care and use of laboratory animals and were approved by the Ethics Review Committee of Animal Experiments, Guizhou University of Traditional Chinese Medicine (Approval No. 20220090; approval date: 1 August 2022). The study is reported in accordance with ARRIVE guidelines.

Informed Consent Statement: Not applicable.

Data Availability Statement: Publicly available datasets (GSE55235, GSE77298, GSE55457, GSE200815 and GSE246416) were analyzed in this study. All the datasets presented in this study can be obtained from the GEO (http://www.ncbi.nlm.nih.gov/geo, accessed on 1 March 2026) database. Additional data that support the findings of this study are available upon reasonable request from the corresponding author.

Acknowledgments: We appreciate the Sangerbox and SRplot platforms for providing support in bioinformatics analysis and plotting, GEO database for providing available data, and Jiuzhang Calculation-Professional Simulation Computing Platform (https://ninecalc.com, accessed on 1 March 2026) for providing powerful computing resources and technical assistance, enabling us to successfully complete this research work and publish this paper.

Conflicts of Interest: The authors declare that they have no known competing financial interests or personal relationships that could have appeared to influence the work reported in this paper.

References

1. Smolen, J.S.; Aletaha, D.; Barton, A.; Burmester, G.R.; Emery, P.; Firestein, G.S.; Kavanaugh, A.; McInnes, I.B.; Solomon, D.H.; Strand, V.; et al. Rheumatoid Arthritis. *Nat. Rev. Dis. Primers* **2018**, *4*, 18001. https://doi.org/10.1038/nrdp.2018.1.
2. Ostrowska, M.; Maśliński, W.; Prochorec-Sobieszek, M.; Nieciecki, M.; Sudoł-Szopińska, I. Cartilage and Bone Damage in Rheumatoid Arthritis. *Reumatologia* **2018**, *56*, 111–120. https://doi.org/10.5114/reum.2018.75523.
3. Kirwan, J. Adverse Effects of Low-Dose Glucocorticoids and DMARD Therapy in Patients with RA—A Complex Relationship? *Nat. Rev. Rheumatol.* **2008**, *4*, 568–569. https://doi.org/10.1038/ncprheum0901.
4. Russu, M.; Lăpuște, V.; Cosău, D.E.; Donica, A.L.; Diaconu, A.-D.; Strugariu, G.; Pomîrleanu, C.; Ancuța, C. Efficacy and Safety of Biologic and Targeted Synthetic DMARDs in Young-Onset Rheumatoid Arthritis: A Systematic Review. *Life* **2026**, *16*, 225. https://doi.org/10.3390/life16020225.
5. Jones, G.; Nash, P.; Hall, S. Advances in Rheumatoid Arthritis. *Med. J. Aust.* **2017**, *206*, 221–224. https://doi.org/10.5694/mja16.01287.
6. Zhao, X.; Zhang, C.; An, Y.; Zhang, Z.; Zhao, J.; Zhang, X.; Yang, Y.; Cao, W. Research on Liver Damage Caused by the Treatment of Rheumatoid Arthritis with Novel Biological Agents or Targeted Agents. *J. Inflamm. Res.* **2023**, *16*, 443–452. https://doi.org/10.2147/JIR.S395137.
7. Smith, M.H.; Gao, V.R.; Periyakoil, P.K.; Kochen, A.; DiCarlo, E.F.; Goodman, S.M.; Norman, T.M.; Donlin, L.T.; Leslie, C.S.; Rudensky, A.Y. Drivers of Heterogeneity in Synovial Fibroblasts in Rheumatoid Arthritis. *Nat. Immunol.* **2023**, *24*, 1200–1210. https://doi.org/10.1038/s41590-023-01527-9.
8. Ospelt, C. Synovial Fibroblasts in 2017. *RMD Open* **2017**, *3*, e000471. https://doi.org/10.1136/rmdopen-2017-000471.
9. Royaei, M.; Tahoori, M.T.; Bardania, H.; Shams, A.; Dehghan, A. Amelioration of Inflammation through Reduction of Oxidative Stress in Rheumatoid Arthritis by Treating Fibroblast-like Synoviocytes (FLS) with DMF-Loaded PLGA Nanoparticles. *Int. Immunopharmacol.* **2024**, *129*, 111617. https://doi.org/10.1016/j.intimp.2024.111617.
10. Neumann, E.; Lefèvre, S.; Zimmermann, B.; Gay, S.; Müller-Ladner, U. Rheumatoid Arthritis Progression Mediated by Activated Synovial Fibroblasts. *Trends Mol. Med.* **2010**, *16*, 458–468. https://doi.org/10.1016/j.molmed.2010.07.004. Erratum in *Trends Mol. Med.* **2011**, *17*, 118.
11. Atzinger, A.; Tascilar, K.; Kleyer, A.; Hueber, A.J.; Schmidkonz, C.; Kuwert, T.; Beck, M.; Fagni, F.; Corte, G.; Ramming, A.; et al. Synovial Fibroblast Activation Occurs before the Onset of Rheumatoid Arthritis and Influences the Risk of Developing Disease. *RMD Open* **2025**, *11*, e005775. https://doi.org/10.1136/rmdopen-2025-005775.
12. Zhang, F.; Jonsson, A.H.; Nathan, A.; Millard, N.; Curtis, M.; Xiao, Q.; Gutierrez-Arcelus, M.; Apruzzese, W.; Watts, G.F.M.; Weisenfeld, D.; et al. Deconstruction of Rheumatoid Arthritis Synovium Defines Inflammatory Subtypes. *Nature* **2023**, *623*, 616–624. https://doi.org/10.1038/s41586-023-06708-y.
13. Alivernini, S.; MacDonald, L.; Elmesmari, A.; Finlay, S.; Tolusso, B.; Gigante, M.R.; Petricca, L.; Di Mario, C.; Bui, L.; Perniola, S.; et al. Distinct synovial tissue macrophage subsets regulate inflammation and remission in rheumatoid arthritis. *Nat. Med.* **2020**, 26, 1295–1306. https://doi.org/10.1038/s41591-020-0939-8.
14. Culemann, S.; Grüneboom, A.; Nicolás-Ávila, J.Á.; Weidner, D.; Lämmle, K.F.; Rothe, T.; Quintana, J.A.; Kirchner, P.; Krljanac, B.; Eberhardt, M.; et al. Locally renewing resident synovial macrophages provide a protective barrier for the joint. *Nature* **2019**, 572, 670–675. https://doi.org/10.1038/s41586-019-1471-1.
15. Wu, D.; Huang, Y.; Zhao, J.; Long, W.; Wang, B.; Wang, Y.; Chen, H.; Wu, R. Synovial Macrophages Drive Severe Joint Destruction in Established Rheumatoid Arthritis. *Sci. Rep.* **2025**, *15*, 12111. https://doi.org/10.1038/s41598-025-93784-x.
16. Zhu, J.; Wei, J.; Lin, Y.; Tang, Y.; Su, Z.; Li, L.; Liu, B.; Cai, X. Inhibition of IL-17 Signaling in Macrophages Underlies the Anti-Arthritic Effects of Halofuginone Hydrobromide: Network Pharmacology, Molecular Docking, and Experimental Validation. *BMC Complement Med. Ther.* **2024**, *24*, 105. https://doi.org/10.1186/s12906-024-04397-2.

17. Zhang, F.; Wei, K.; Slowikowski, K.; Fonseka, C.Y.; Rao, D.A.; Kelly, S.; Goodman, S.M.; Tabechian, D.; Hughes, L.B.; Salomon-Escoto, K.; et al. Defining Inflammatory Cell States in Rheumatoid Arthritis Joint Synovial Tissues by Integrating Single-Cell Transcriptomics and Mass Cytometry. *Nat. Immunol.* **2019**, *20*, 928–942. https://doi.org/10.1038/s41590-019-0378-1.
18. Croft, A.P.; Campos, J.; Jansen, K.; Turner, J.D.; Marshall, J.; Attar, M.; Savary, L.; Wehmeyer, C.; Naylor, A.J.; Kemble, S.; et al. Distinct Fibroblast Subsets Drive Inflammation and Damage in Arthritis. *Nature* **2019**, *570*, 246–251. https://doi.org/10.1038/s41586-019-1263-7. Correction in *Nature* **2026**, 649, E2.
19. Li, Y.; Zhang, N.; Peng, X.; Ma, W.; Qin, Y.; Yao, X.; Huang, C.; Zhang, X. Network Pharmacology Analysis and Clinical Verification of Jishe Qushi Capsules in Rheumatoid Arthritis Treatment. *Medicine* **2023**, *102*, e34883. https://doi.org/10.1097/MD.0000000000034883.
20. Hanlon, M.M.; Smith, C.M.; Canavan, M.; Neto, N.G.B.; Song, Q.; Lewis, M.J.; O'Rourke, A.M.; Tynan, O.; Barker, B.E.; Gallagher, P.; et al. Loss of Synovial Tissue Macrophage Homeostasis Precedes Rheumatoid Arthritis Clinical Onset. *Sci. Adv.* **2024**, *10*, eadj1252. https://doi.org/10.1126/sciadv.adj1252.
21. Floudas, A.; Smith, C.M.; Tynan, O.; Neto, N.; Krishna, V.; Wade, S.M.; Hanlon, M.; Cunningham, C.; Marzaioli, V.; Canavan, M.; et al. Distinct Stromal and Immune Cell Interactions Shape the Pathogenesis of Rheumatoid and Psoriatic Arthritis. *Ann. Rheum. Dis.* **2022**, *81*, 1224–1242. https://doi.org/10.1136/annrheumdis-2021-221761.
22. Edalat, S.G.; Gerber, R.; Houtman, M.; Lückgen, J.; Teixeira, R.L.; Palacios Cisneros, M.D.P.; Pfanner, T.; Kuret, T.; Ižanc, N.; Micheroli, R.; et al. Molecular Maps of Synovial Cells in Inflammatory Arthritis Using an Optimized Synovial Tissue Dissociation Protocol. *iScience* **2024**, *27*, 109707. https://doi.org/10.1016/j.isci.2024.109707.
23. Konishi, H.; Kanou, S.-E.; Yukimatsu, R.; Inui, M.; Sato, M.; Yamamoto, N.; Nakano, M.; Koshiba, M. Adenosine Inhibits TNFα-Induced MMP-3 Production in MH7A Rheumatoid Arthritis Synoviocytes via A2A Receptor Signaling. *Sci. Rep.* **2022**, *12*, 6033. https://doi.org/10.1038/s41598-022-10012-6.
24. Lindy, O.; Konttinen, Y.T.; Sorsa, T.; Ding, Y.; Santavirta, S.; Ceponis, A.; Lopez-Otin, C. Matrix Metalloproteinase 13 (Collagenase 3) in Human Rheumatoid Synovium. *Arthritis Rheum*. **1997**, *40*, 1391–1399. https://doi.org/10.1002/art.1780400806.
25. Konttinen, Y.T.; Salo, T.; Hanemaaijer, R.; Valleala, H.; Sorsa, T.; Sutinen, M.; Čeponis, A.; Xu, J.-W.; Santavirta, S.; Teronen, O.; et al. Collagenase-3 (MMP-13) and Its Activators in Rheumatoid Arthritis: Localization in the Pannus-Hard Tissue Junction and Inhibition by Alendronate. *Matrix Biol.* **1999**, *18*, 401–412. https://doi.org/10.1016/S0945-053X(99)00030-X.
26. Ma, K.; Miao, L.; Li, B.; Yu, W.; Liu, F.; Liu, K.; Li, Y.; Huang, C.; Yang, Z. Mechanism of Action of Nrf2 and Its Related Natural Regulators in Rheumatoid Arthritis. *J. Orthop. Surg. Res.* **2024**, *19*, 759. https://doi.org/10.1186/s13018-024-05221-w.
27. Zhang, L.; Huang, X.; Xiong, H.; Yang, L. The Nrf2/HO-1 Signaling Pathway in Arthritis: From Molecular Mechanisms to Therapeutic Potential. *Front. Cell Dev. Biol.* **2026**, *14*, 1728679. https://doi.org/10.3389/fcell.2026.1728679.
28. Tan, Y.; Buch, M.H. "Difficult to Treat" Rheumatoid Arthritis: Current Position and Considerations for next Steps. *RMD Open* **2022**, *8*, e002387. https://doi.org/10.1136/rmdopen-2022-002387.
29. Bersuker, K.; Hendricks, J.M.; Li, Z.; Magtanong, L.; Ford, B.; Tang, P.H.; Roberts, M.A.; Tong, B.; Maimone, T.J.; Zoncu, R.; et al. The CoQ Oxidoreductase FSP1 Acts Parallel to GPX4 to Inhibit Ferroptosis. *Nature* **2019**, 575, 688–692. https://doi.org/10.1038/s41586-019-1705-2

Disclaimer/Publisher's Note: The statements, opinions and data contained in all publications are solely those of the individual author(s) and contributor(s) and not of MDPI and/or the editor(s). MDPI and/or the editor(s) disclaim responsibility for any injury to people or property resulting from any ideas, methods, instructions or products referred to in the content.